When is it too Late to Brake?

Yang Chen
Research Scientist,
Center for Vehicle Systems and Safety, Virginia Tech, VA

Zichen Zhang
Research Assistant,
Center for Vehicle Systems and Safety, Virginia Tech, VA

Campbell Neighborgall
Research Assistant,
Center for Vehicle Systems and Safety, Virginia Tech, VA

Mehdi Ahmadian*
J. Bernard Jones Chair and Director,
Center for Vehicle Systems and Safety, Virginia Tech, VA
Email: ahmadian@vt.edu
*Corresponding author

Abstract: This paper provides a simulation analysis of the braking action that would prevent untripped rollovers of long combination vehicles (LCV) in turns when the entry speed into a turn exceeds the vehicle's threshold. A co-simulation model is used to integrate the details of truck pneumatic brakes (developed in Simulink®) in a TruckSim® model. The models are validated with field-test data. Using the validated models, various braking initiation times (relative to the start of steering) are performed for a 150-ft J-turn. The simulation results reveal that at higher speeds, there is very little time for the driver to initiate braking before it is too late to avoid a rollover, referred to as Critical Brake Initiation Time (CBIT). For instance, at an entry speed of 40 mph (64 km/hr), applying the brakes for a fully-loaded truck beyond 1.0s would not prevent a rollover. The results also indicate increasing the speed by 25% from 40 mph (64 km/hr) to 50 mph (80 km/hr), reduces CBIT by 90%, from 1.0s to 0.1s. The effect of cargo load on CBIT is less dramatic than speed. At 40 mph (64 km/hr), increasing the cargo load by 47%, from 15000 lb. (6800 kg) to 22000 lb. (10000 kg), decreases the CBIT by 17%, from 1.2s to 1.0s.

Keywords: long combination vehicles; LCV; rollover; braking; steering, A-double; brake initiation; brake model; roll stability; yaw stability

1. Introduction

Rollover risk posed by long combination vehicles (LCVs) has drawn increasingly more attention over the past decades [1, 2]. Given the large size and elevated center-of-gravity (CG) of LCVs, as is well known, they are more susceptible to rollovers than cars and small trucks [3]. LCV rollovers are more likely to result in severe injuries and property damage [4]. According to the data

published by the Federal Motor Carrier Safety Administration (FMCSA) [5], in 2018, large-truck-related rollover accounted for 4000 injury crashes and 186 fatal crashes in the U.S. . A summary of accident statistics compiled by the Insurance Institute for Highway Safety (IIHS) indicates that the occupant-death rate of large-truck rollovers is 125% higher than that for cars [6]. In particular, 74% of the occupant deaths in large vehicle crashes are associated with combination trucks [6].

An LCV rollover event in turns during highway driving is principally attributed to three events: (1) exceeding the lateral acceleration limit (referred to as the "untripped rollover") [7]; (2) the traveling off of the paved roadway onto uneven terrain (hence, triggering a terrain-induced rollover) [8], and; (3) losing control and sliding sideway into a roadside obstacle such as a curb or guardrail [9]. Reducing speed through timely braking can reduce the likelihood of these incidents, particularly the untripped rollovers [10, 11]. Timely braking slows the vehicle, which in turn reduces lateral acceleration and maintains the rollover stability of the vehicle. If, however, the driver does not have sufficient time to react to the obstacle ahead or initiates braking too late, the lateral accelerations could exceed the rollover threshold, causing the vehicle to rollover. Late braking could also cause excessive outward sway of the rear most trailer, posing a risk of pulling onto the shoulder or colliding with a roadside guardrail. This could induce a terrain-induced or tripped rollover [12]. For the sake of brevity, this study will consider the speed-induced untripped rollovers that are most prevalent among LCVs, i.e., the event (1) mentioned above.

Braking on time is of great importance in stopping speed-induced rollover accidents. It, however, is difficult for the driver to sense the excessive speed for his roll stability and reduce speed through braking because of the lack of any advance notice he may have. Rollovers often occur quickly. The vehicle may tip over and start rolling over before the driver even realizes the pending rollover. The separation between the tractor cab and trailers, along with the higher CG of the trailers (relative to the tractor) reduces the driver's ability to sense the roll movements of the trailer(s) [13]. Often the driver does not have an opportunity to apply the brakes until it is too late, because of the lack of any warning. This is particularly true for heavy trucks and LCVs.

Studying the timing of braking for avoiding rollover accidents is of great interest. Such studies are strongly tied to highway safety and are especially helpful in the development of LCV rollover prevention systems, including rollover warning systems (signaling the driver to apply the brakes), roll stability control (RSC), and electronic stability control (ESC) systems [14-16]. Although some

studies have considered tractor-semitrailers with a single trailer, there are not many studies for LCVs such as double 28-ft and 33-ft trailers that are operating with increasing frequency on the U.S. highways. This study is aimed at evaluating the braking action that is needed for preventing rollovers, using a detailed model of the pneumatic brake dynamics in a reasonably accurate truck dynamics model. The brake dynamics are modeled in Simulink® and merged with a high-order multi-body dynamics model in TruckSim®, an accepted simulation tool for commercial vehicles.

2. LCV Configuration and Literature Review

There exist various types of LCVs (hauling different combinations and sizes of multiple trailers), depending on the need of the fleet that operates them [17, 18]. This study is focused on trucks with A-double trailers of 33-ft length, which are operating with increasing frequency on U.S. highways. As shown in Figure 1, this type of LCV is also called a 33-ft A-double since the two semi-trailers are connected by an A-shaped dolly. As stated in a report from the Americans for Modern Transportation [19] provides increased cargo volume capacity (in comparison with conventional 28-ft A-doubles) and there has been significant interest by fleets in using them, hence the reason for considering them in this study.

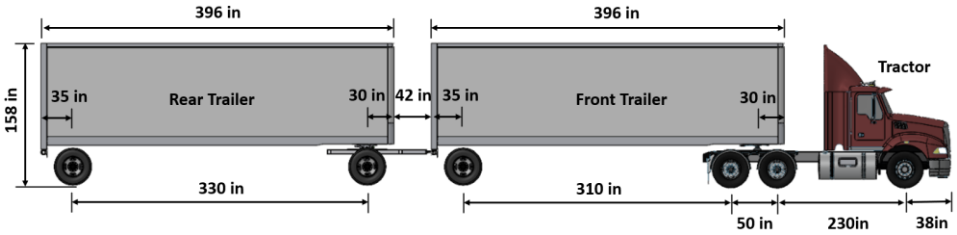

Figure 1. 33-ft double-trailer with A-dolly connecter, commonly referred to as “33-ft A-double”

There have been very few studies [20-22] on the effect of braking on lateral dynamic characteristics of commercial trucks. Some past studies indicate that in conditions of braking and cornering simultaneously, the relationship between the tire longitudinal force and lateral force can be simply described by the friction-ellipse theory [7, 23-25]. During combined braking and steering, there is a higher likelihood of contact patch saturation due to combined lateral and longitudinal forces, which leads to a higher likelihood of loss of traction and more complex dynamics. In a recent study by Shaohua et al. [26], the influence of braking on yaw and roll stability of straight trucks in cornering braking conditions is examined, using a 23-degrees-of-freedom (DOF) dynamic model. In their study, braking is found to assist in improving the yaw and roll stability of the vehicle. Their research also shows that the rollover critical speed is lower than the

yaw critical speed for a straight truck (i.e., on dry pavement the truck is more prone to rollover than spinning out or becoming grossly understeered). In addition, Zhang et al. [27] performed a simulation study on combined braking and evasive steering maneuver for a logging semitruck, indicating that the vehicle's response to evasive steering decreases with increased braking force.

In this paper, we extend the previous studies by providing a simulation-based investigation on the combined braking and steering maneuvers for 33-ft A-doubles. In particular, the critical brake initiation time (CBIT) to avoid a rollover while also avoiding striking roadside objects such as guard rails that could induce a tripping hazard. The study is performed for a 150-ft J-turn at various speeds and loading conditions.

3. LCV Dynamics Model Development

For this study, a multi-body dynamics model with 36 degrees-of-freedom for the 33-ft A-double is developed in TruckSim® [1, 28-31]. The LCV model in TruckSim® considers the lateral, longitudinal, vertical, roll, yaw, and pitch motions (6 degrees-of-freedom) of the sprung mass, and the vertical and roll motions (2 degrees-of-freedom) of the unsprung mass for each axle of the tractor, front trailer, dolly, and rear trailer in an LCV with two trailers and a convertor A-dolly (commonly referred to as "A-double"). The tractor and dolly are connected to the front and rear trailers, respectively, by fifth wheel hitches, which are modeled as a joint with free yaw rotation and limited roll and pitch rotation. The LCV model also considers the non-linear dynamics of the pneumatic suspensions on the tractor drive axles, trailers axles, and dolly axle. The tractor steer axle is equipped with a leaf spring (or mechanical) suspension. The fluid dynamic equations from prior studies by the authors, [28, 32], are integrated into TruckSim® model to represent the details of the dynamic behaviors of airsprings. The airsprings are modeled as closed compliant vessels in which no air flows in or out of them at the ride height, but their internal pressure changes as a function of the suspension stroke. The dimensional parameters, such as wheelbase, track, suspension lateral spacing, etc., are determined from measurements on a 33-ft A-double available at the Virginia Tech's Center for Vehicle Systems and Safety (CVeSS). All of the model parameter values are included in Table A1 of the Appendix A.

Here, particular attention is paid to the trailer CG inertial properties and tire force characterization that are important to accurately modeling the combined dynamics of steering and braking. The coupled Simulink®-Trucksim® model is calibrated and validated using test data. For additional

accuracy, the model includes a detailed pneumatic braking dynamic model that is used in place of the default TruckSim® brake model. Specifically, a pneumatic brake model is developed in Simulink® (in Section 3.4) and coupled with TruckSim® through a co-simulation technique (in Section 3.5) to predict the effect of pneumatic braking on LCV dynamics more precisely.

3.1 Trailer CG Inertial Properties Determination

To determine trailer CG properties, a CAD model of the 33-ft trailer is constructed in SolidWorks®. The model includes detailed structural components, axle/wheel assembly. Each trailer is loaded with 15000 lb., which represents the average weight that these types of trailers typically carry. The load is uniformly distributed while occupying 80% of the trailer's inner volume. The trailer CG and inertial parameters determined from the CAD model (shown in Table 1) are used for the TruckSim® model.

Table 1. Trailer CG inertial parameters determined from the SolidWorks model

Parameters	**Value**
Trailer tare weight	10100 lb.
Loaded trailer weight	25100 lb.
Loaded vehicle CG height to the ground	79.5 in
Loaded vehicle CG to the kingpin	183.5 in
Roll moment of inertia	403219 lb.·ft^2
Pitch moment of inertia	2990579 lb.·ft^2
Yaw moment of inertia	2913493 lb.·ft^2

3.2 Tire Force Characterization

The tire longitudinal traction is mainly dependent on the slip ratio, the normalized difference between the tire forward speed ωR_t, and the vehicle forward speed, v_x [33]:

$$\kappa = \frac{\omega R_t - v_x}{v_x} \tag{1}$$

To model the tire longitudinal traction and braking characteristics, a look-up table is developed based on the test results in Figure 2 for a "typical" truck tire [34]. The longitudinal force increases with the slip ratio until κ_{max} where the peak longitudinal force occurs. Beyond κ_{max} , longitudinal traction force decreases with increasing slip ratio until wheel spin (lock up, in case of braking) is reached. Traction and braking forces increase with increasing wheel load.

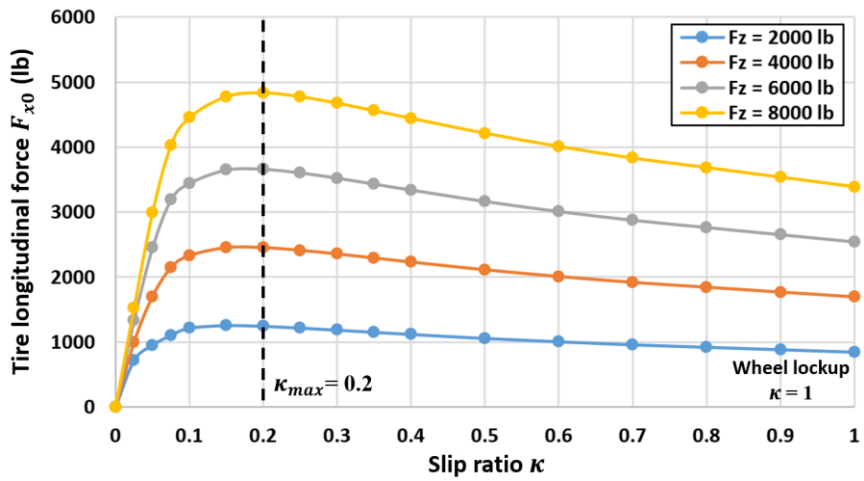

Figure 2. Test data of truck tire longitudinal force versus slip ratio [34]

The lateral (steering) forces have similar characteristics to the longitudinal forces. They can be modeled as a non-linear function of the slip angle (the angle between the tire's travel direction and its heading) [33] and [35]:

Tire slip angle of steer axle left side: $\alpha_{sl} = tan^{-1}(\frac{v_y+\dot{\theta}a}{v_x-\dot{\theta}c/2}) - \delta$ (2)

Tire slip angle of steer axle right side: $\alpha_{sr} = tan^{-1}(\frac{v_y+\dot{\theta}a}{v_x+\dot{\theta}c/2}) - \delta$ (3)

Tire slip angle of rear axle left side: $\alpha_{rl} = tan^{-1}(\frac{v_y-\dot{\theta}b}{v_x-\dot{\theta}c/2})$ (4)

Tire slip angle of rear axle right side: $\alpha_{rr} = tan^{-1}(\frac{v_y-\dot{\theta}b}{v_x+\dot{\theta}c/2})$ (5)

where δ is the steering angle (at the road wheel), v_x and v_y are the vehicle's longitudinal and lateral velocities, $\dot{\theta}$ is the yaw rate of the vehicle, a and b are CG distance to the front and rear axles, and c is the track width.

Similar to the longitudinal traction, the test results in Figure 3 for a 11R22.5 tire are used to develop a look-up table for the lateral forces [36]. The longitudinal and lateral characteristics of the tire are integrated into TruckSim® in place of the canned tire models that are available in the software. As shown in Figure 3, the lateral forces increase with increasing slip angle and reach their maximum at approximately 14 degrees (i.e., α_{max}= 14 deg). After the peak, the lateral forces begin to decrease with increasing slip angle.

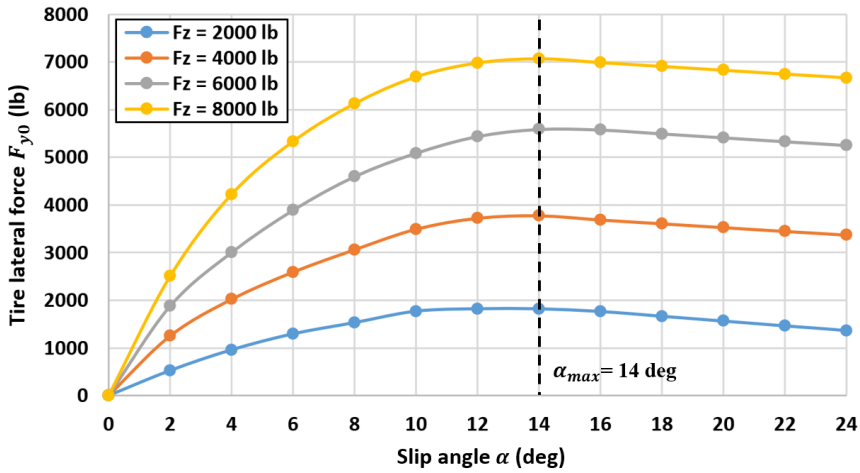

Figure 3. Test data of truck tire lateral force versus slip angle [36]

During combined steering and braking, the tire experiences both longitudinal and lateral forces. A non-linear tire model proposed by Pacejka [37-39] is used in this study to model the tire force characteristics for combined steering and braking:

$$F_x = \begin{cases} [F_{x0} - \sigma^*(F_{x0} - F_{y0})\left(\frac{\sigma_y{}^*}{\sigma^*}\right)^2]cos\beta & for\ \sigma^* \leq 1 \\ [F_{x0} - (F_{x0} - F_{y0})\left(\frac{\sigma_y{}^*}{\sigma^*}\right)^2]cos\beta & for\ \sigma^* > 1 \end{cases} \tag{6}$$

$$F_y = \begin{cases} [F_{y0} - \sigma^*(F_{y0} - F_{x0})\left(\frac{\sigma_x{}^*}{\sigma^*}\right)^2]cos\beta & for\ \sigma^* \leq 1 \\ [F_{y0} - (F_{y0} - F_{x0})\left(\frac{\sigma_x{}^*}{\sigma^*}\right)^2]cos\beta & for\ \sigma^* > 1 \end{cases} \tag{7}$$

where F_{x0} and F_{y0} are the tire longitudinal and lateral forces discussed earlier. σ_x and σ_y are the longitudinal and lateral slip ratios, calculated by:

$$\sigma_x = \frac{\kappa}{1+\kappa} \tag{8}$$

$$\sigma_y = \frac{tan\,\alpha}{1+\kappa} \tag{9}$$

where κ is the slip ratio and α is the slip angle. Normalizing the composite slip ratios with respect to the maximum slip ratio yields:

$$\sigma_x{}^* = \frac{\sigma_x}{\sigma_{xm}} = \frac{\sigma_x(1+k_{max})}{k_{max}} = \frac{\kappa(1+k_{max})}{k_{max}(1+\kappa)} \tag{10}$$

$$\sigma_y{}^* = \frac{\sigma_y}{\sigma_{ym}} = \frac{\sigma_y(1+\kappa)}{tan\alpha_{max}} = \frac{tan\,\alpha}{tan\alpha_{max}} \tag{11}$$

where $\sigma_x{}^*$ and $\sigma_y{}^*$ are the maximum normalized composite slip ratios in the longitudinal and lateral directions, κ_{max} is the slip ratio at the peak longitudinal force (in Figure 2), and α_{max} is the value of the slip angle at the peak lateral force (in Figure 3). The magnitude of the slip ratio at the contact patch is:

$$\sigma^* = \sqrt{\sigma_x{}^{*2} + \sigma_y{}^{*2}} \tag{12}$$

The sideslip angle β in Equations (6) and (7) is calculated according to:

$$\beta = tan^{-1}\frac{\sigma_y{}^*}{\sigma_x{}^*} + \frac{2(tan^{-1}\frac{\sigma_y}{\sigma_x} - tan^{-1}\frac{\sigma_y{}^*}{\sigma_x{}^*})}{\pi}\tan^{-1}(1.1\sigma^{*2}) \tag{13}$$

Using Pacejka's tire model, the changes in tire longitudinal and lateral forces as a result of the slip ratio for different slip angles, α, can be determined, as shown in Figure 4 for tire load = 4000 lb. The increase in slip ratio results in a decrease in the tire lateral force at a given slip angle. The application of the slip ratio causes an increase in the longitudinal force, followed by a reduction. Furthermore, a larger deviation is observed between the tire longitudinal and lateral forces as the sideslip angle decreases. The findings agree with the studies by Gillespie [33] and Morrison [20].

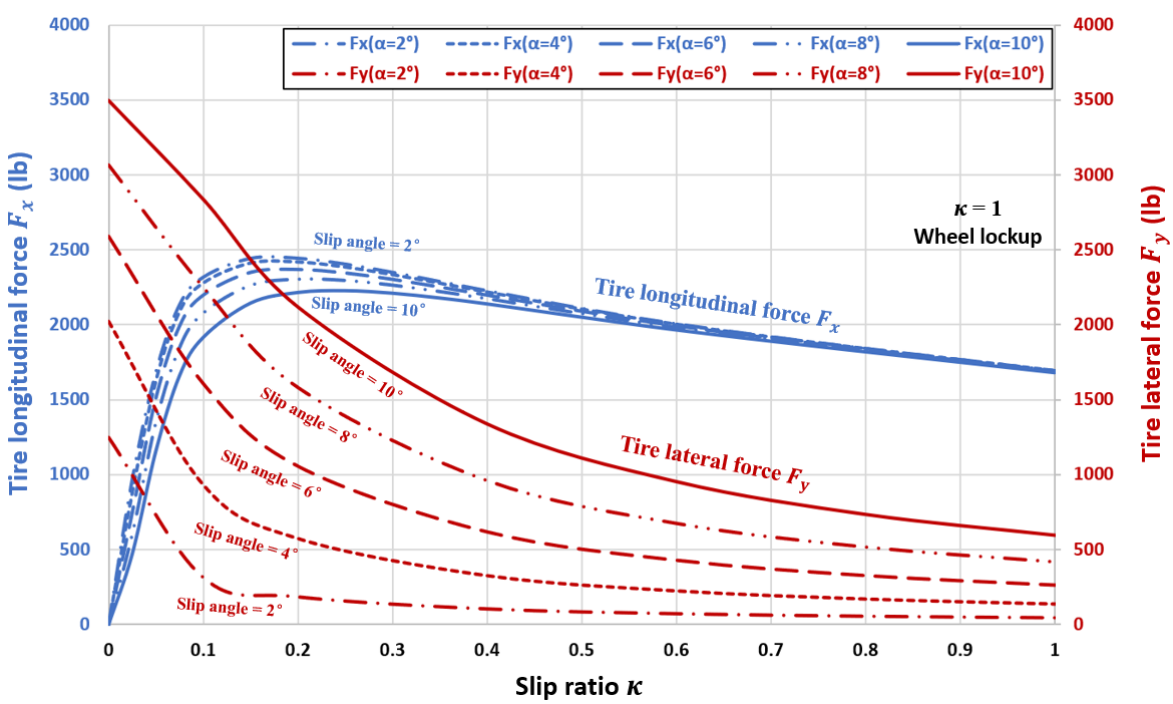

Figure 4. Tire longitudinal and lateral forces versus the slip ratio based on the Pacejka tire model

3.3 Pneumatic Brake Subsystem Model

A schematic layout of a pneumatic brake system in a 33-ft A-double is shown in Figure 5. Upon braking, air is drawn from the air reservoir through the treadle valve and is delivered to the brake chambers of the steering axle, while passing on to the relay valves for the drive axle(s) and trailer(s) axles through the control line shown in red in Figure 5. The pressurized air in the control line signals the relay valve to charge the brake chambers from the brake reservoirs (marked in blue in Figure 5). The air pressure in the brake chamber pushes out the pushrod and presses the brake pads against the rotating drum to slow down the wheel rotation [40]. To reasonably simulate the complex braking dynamics, a pneumatic brake subsystem model is developed in Simulink® and integrated into TruckSim®. The details of the brake modeling that includes the brake delays and other effects present in LCVs are described in an earlier paper by the authors [41]. For brevity, the details of the brake model that is integrated into the co-simulation model are not included here. A high-level description of the model is included in Appendix B.

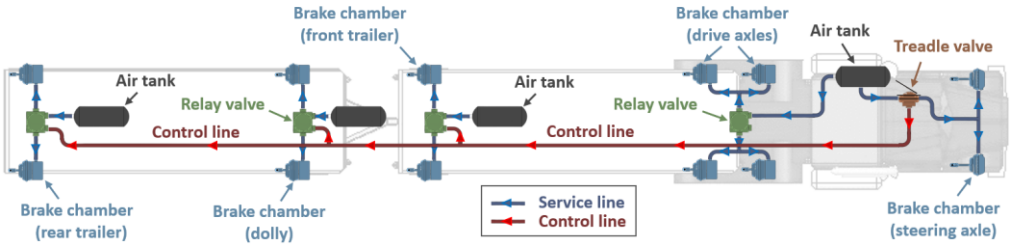

Figure 5. Schematic representation of a pneumatic brake system for a 33-ft A-double (top view)

4. Vehicle Dynamic Model Validation

The LCV dynamic model is validated using test data from braking-in-turn maneuvers on an identical 33-ft A-double truck. The tests were conducted at the Transportation Research Center (East Liberty, OH) by the Center for Vehicle Systems and Safety at Virginia Tech. The LCV was instrumented with pressure transducers mounted at the inlet ports of the brake chambers to detect change in braking pressure of the tractor and trailers. In addition, accelerometers were installed at the CG position of the tractor and trailers for measuring longitudinal and lateral accelerations. The test vehicle was equipped with a GPS sensor for recording and control of the driving speed.

The model is validated by comparing its simulation results with the test data collected from a braking-in-turn maneuver at the entering speed of 35 mph (56 km/hr). The steering and braking

robots shown in Figure 6 are used to maintain consistency and control during the tests. The steering robot is a shaft-mounted assembly that is controlled remotely by an operator. It provides a precise steering angle during each maneuver. The braking robot is a pedal-mounted pneumatic actuator that controls the pedal movement with high precision. It is used to apply hard braking, mild braking, etc. in a controlled manner. The steering and braking robots are coordinated to allow precise steering and braking actions for the tests; for example, as shown in Figure 7. The braking shown in Figure 7 is classified as hard braking. The control line's brake pressure rises from approximately 0 to 85 psi in 0.2s, according to FMVSS 121 requirement [42]. A steering angle of 210 degrees is initiated 1.5s earlier than braking by the steering robot. The relative delay between steering and braking is changed to determine the threshold of braking action in a turn and mark the time when braking is not able to scrub speed sufficiently to eliminate tip-up or rollover (i.e., reaching the point of "too late to brake.")

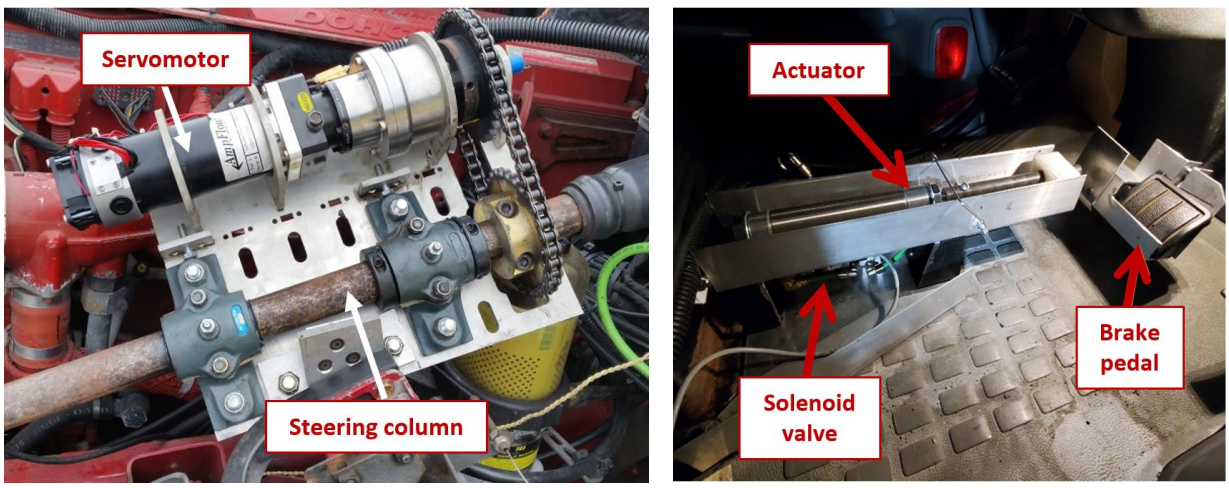

(a) (b)

Figure 6. (a) Steering and (b) braking robots used in the truck field testing

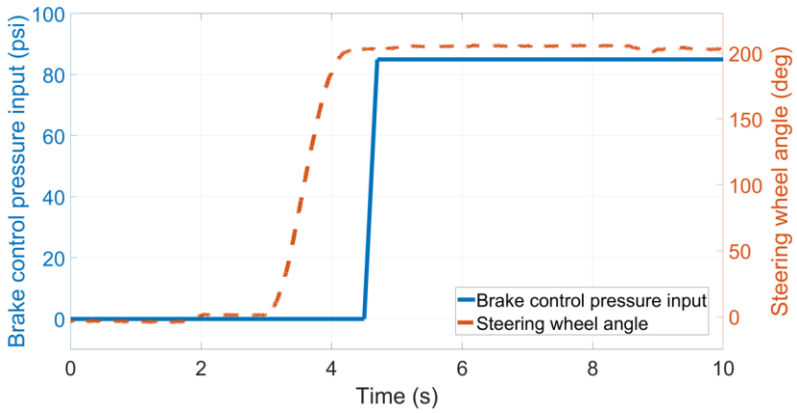

Figure 7. Steering and braking inputs used for the field tests and simulation model

Figures 8 and 9 provide a comparison between the modeling results and test data for brake pressure, speed, and tractor and trailers' longitudinal deceleration and lateral acceleration. They also compare the modeling and test results for the articulation angles between the two trailers and the front trailer and tractor. As shown in Figure 8, upon applying the brakes, the chamber pressure at each wheel rises from zero to its final pressure (85 psi, for this study) with a delay due to the hoses and valves. The model successfully captures the brake delays and transient pressure changes for all chambers, including when the ABS activates. This is critical for accurately representing the brake dynamics in the TruckSim® model.

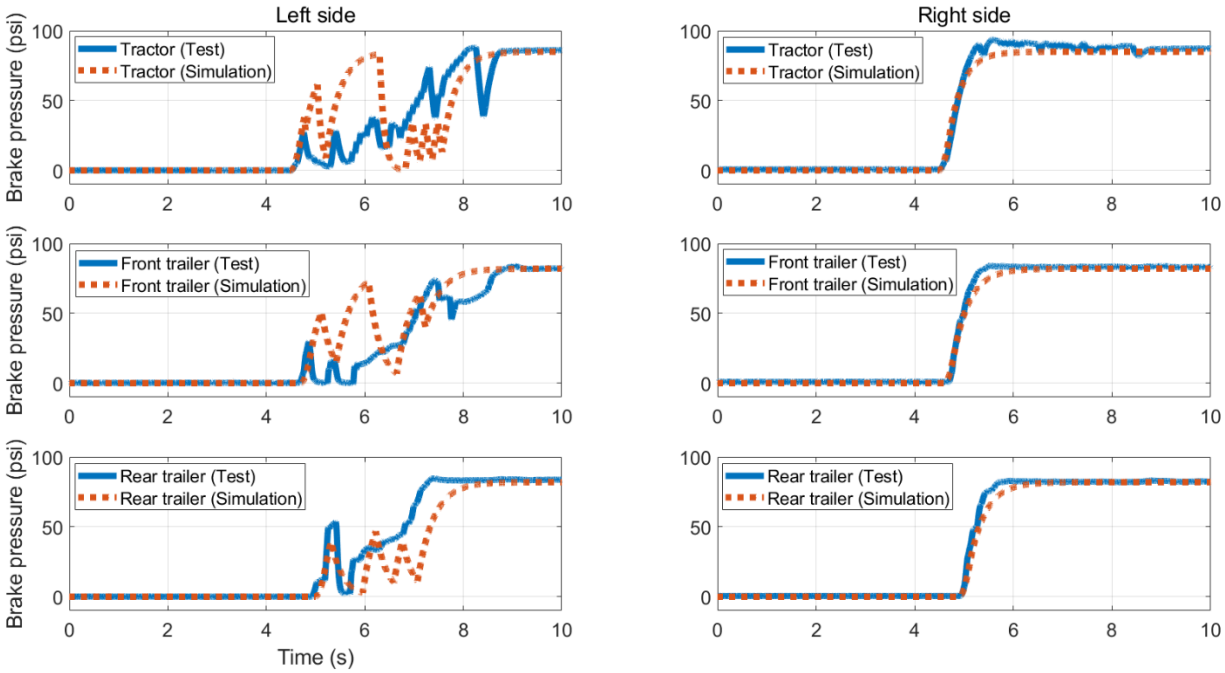

Figure 8. Comparison of brake pressures between modeling results and test data

The simulation output also agrees well with the test data, in terms of the reduction in speed due to braking (Figure 9a), forward deceleration (Figure 9b), articulation angles at the front and rear of the lead trailer (Figure 9c), and lateral acceleration (Figure 9d). This confirms the capability of the model to accurately predict the dynamic behavior of the A-double trucks during steering and braking maneuvers of the type commonly arising during highway driving or accident avoidance. It should be noted that some small unavoidable differences are observed between the simulation and test results when the ABS is activated due to loss of wheel load on one side. These differences are primarily due to the estimation of the ABS proprietary software on the test truck that is not known to us. Other factors that could contribute, to a lesser degree, are steering losses, tire wear,

wind, etc. that are present in the test results but cannot be accurately reflected in the simulation model. Collectively, these factors cause the differences observed in Figure 8 for the ABS activation time and brake pressure fluctuations when ABS is activated on the left side of the vehicle.

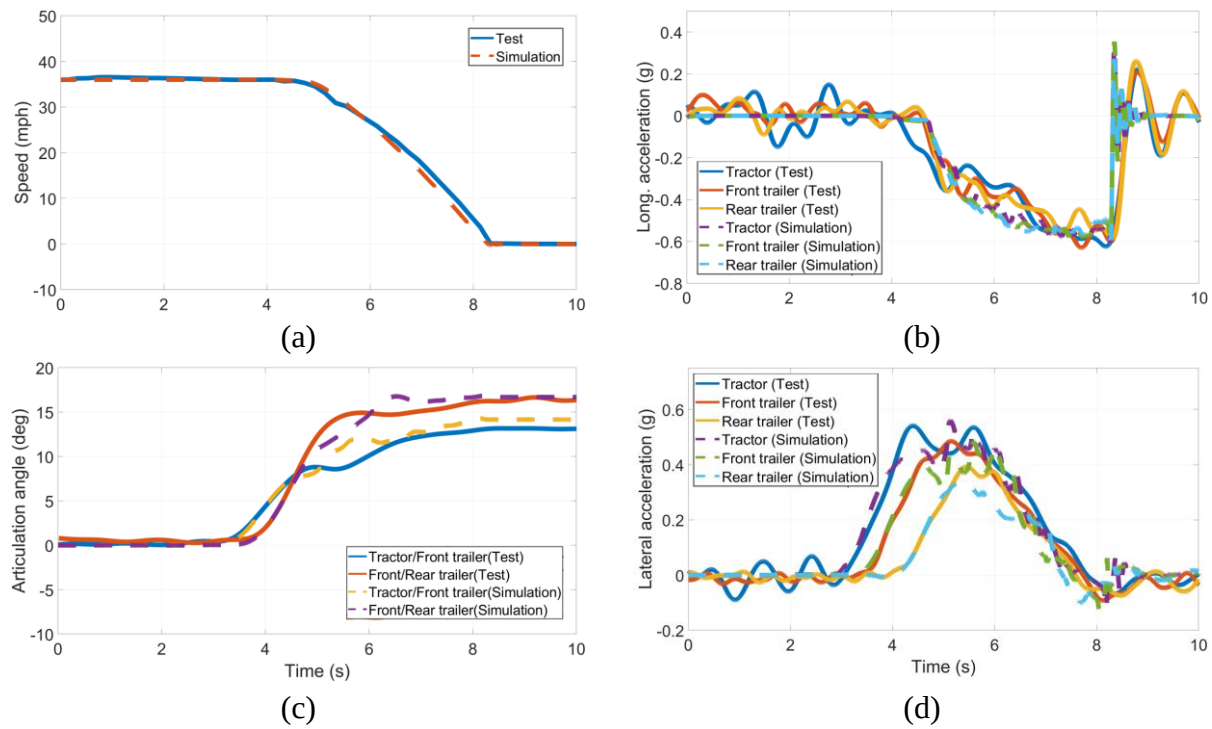

Figure 9. Comparison between modeling results and test data; (a) speed reduction; (b) longitudinal (forward) deceleration; (c) articulation angles; (d) lateral acceleration.

5. Simulation Study

Using the validated model, an extensive series of simulations are conducted to assess the influence of brake initiation time (BIT) on LCV propensity to roll over; specifically, as it relates to the critical brake initiation time (CBIT) of rollover. The brake initiation time (BIT) is the period from the steering start (t_{steer}) to the braking start (t_{brake}):

$$Brake\ Initiation\ Time\ (BIT) = t_{brake} - t_{steer} \tag{14}$$

A larger BIT implies a larger time lapse between steering and braking. BIT=0 implies no lapse between steering and braking. Since it is assumed in this study that braking always occurs after steering, BIT is never negative. The 150-ft J-turn maneuver shown in Figure 10 emulating highway exit-ramps is adopted for the study. For a common 12-ft highway lane, it is assumed that the truck's steer axle center travels along the centerline of the lane [43]. Other assumptions are:

- Aerodynamics drag is negligible
- The dry asphalt roadway is flat and has a coefficient of friction = 0.8 [44]
- The driver perception/reaction time, braking delay, and steering delay are not included, and they must be added to the results discussed later (this is mainly to make the results more universe since different studies assume different driver perception/reaction times and steering and barking delays)
- The electronic stability control system (ESC) and roll stability control system (RSC) do not engage during the maneuvers

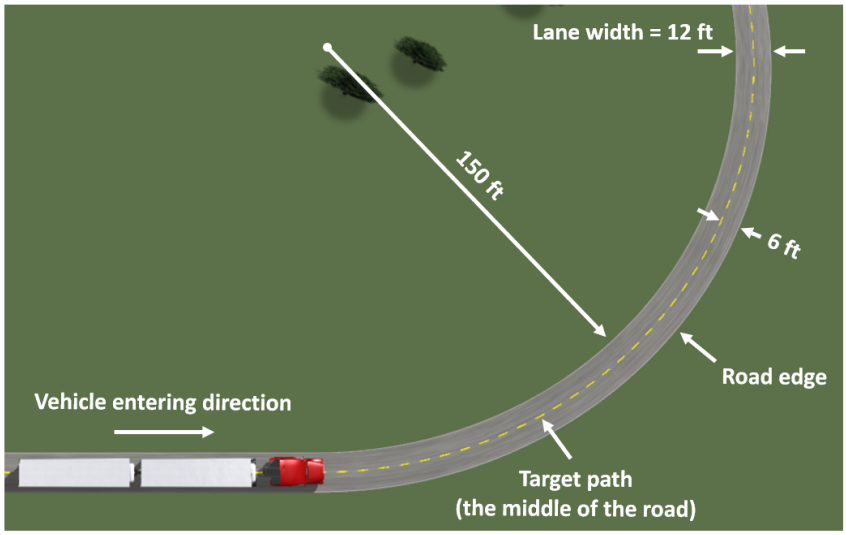

Figure 10. 150-ft J-turn emulating a highway exit ramp

5.1 Braking-in-turn Maneuver (Speed =40 mph (64 km/hr) and BIT =1s)

In this section, a preliminary simulation is performed for the braking-in-turn maneuver at the initial speed of 40 mph (64 km/hr) and the BIT of 1s, as shown in Figure 11. The purpose of the preliminary study is to provide an estimate of the speeds and critical brake initiation times (CBIT) that would cause rollovers. The estimates are then used for conducting tests that start outside of the rollover time and CBIT thresholds, but successively approach the threshold in order to determine the exact effect of CBIT at each speed, and similarly speed at each CBIT. To simulate emergency stopping conditions while steering, hard braking is applied during which the brake control pressure is increased to 85 psi in 0.2 seconds, as per FMVSS 121 [42].

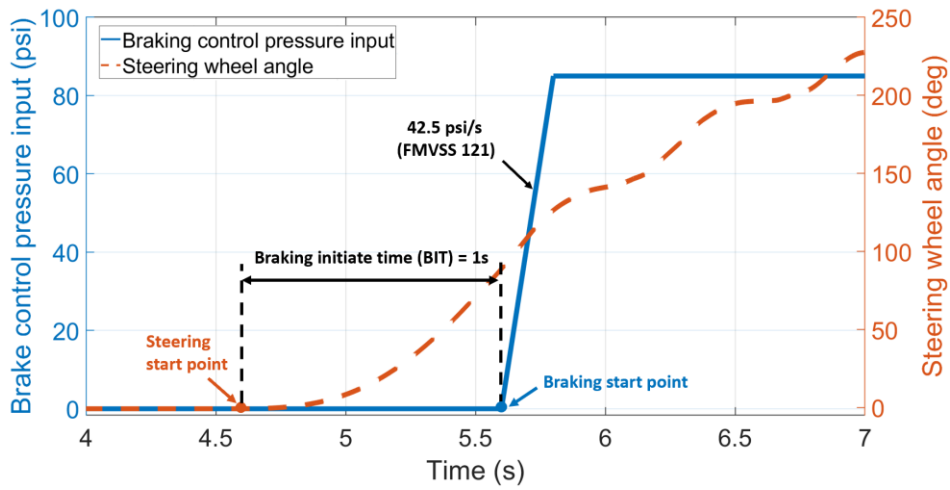

Figure 11. The braking-in-turn maneuver with the BIT of 1s

5.1.1 Braking and Vehicle Longitudinal Dynamics in Braking-in-turn Maneuver

Figure 12 presents the simulation results of the brake chamber pressures for the tractor and two trailers, on the left and right. A close inspection of the figure shows that the rear trailer experiences the largest amount of time delay in generating brake pressure, followed by the front trailer, which is in line with our expectations.

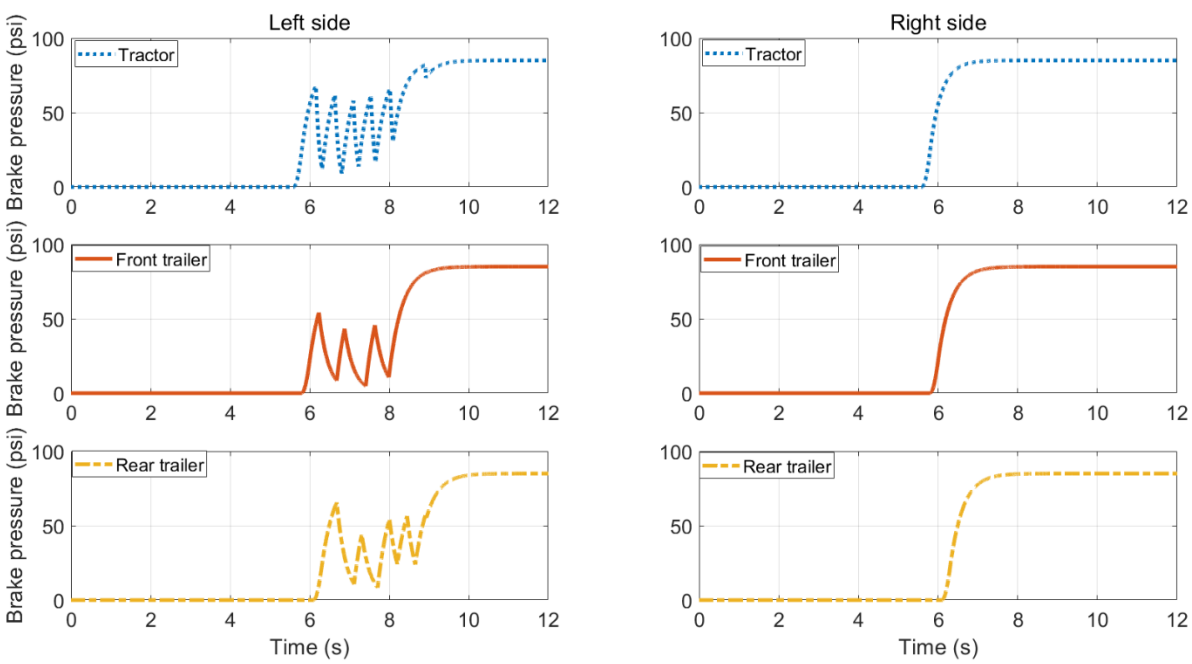

Figure 12. Time trace of brake pressures of the tractor and trailers during the braking-in-turn maneuver (initial speed=40 mph (64 km/hr); BIT $= 1s$)

Furthermore, there is a fluctuation in the brake pressure due to the ABS, which occurs on the left side, because of its lighter dynamic wheel load and higher propensity to lock up in a left-hand turn. The right side (the side to the outside of the turn) does not experience any lock-ups and ABS activation. The brake pressures reach 85 psi at slightly different times for the tractor and trailers, with the right side reaching the steady-state pressure sooner than the left side for each. The longitudinal decelerations and driving speed vs. time during braking are shown in Figures 13. In Figure 13a, the tractor and trailers exhibit almost the same change in longitudinal deceleration, rising quickly and staying around 0.5g to 0.6g until the vehicle stops. The change in speed is nearly linear with time, as shown in Figure 13b.

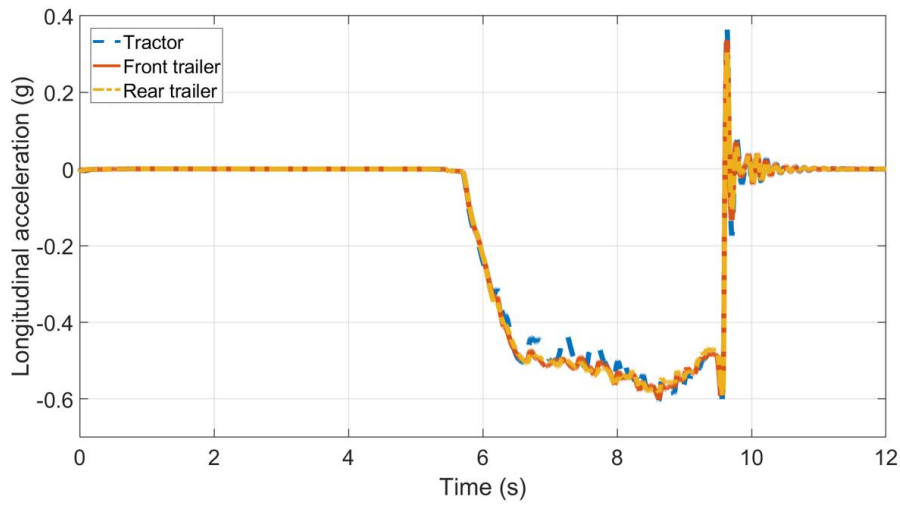

(a)

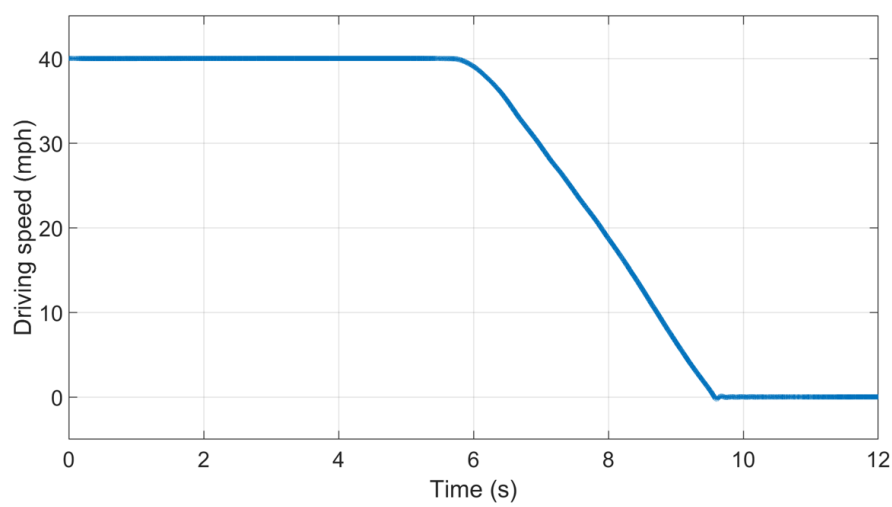

(b)

Figure 13. Time trace of (a) longitudinal accelerations and (b) speed during the braking-in-turn maneuver (initial speed=40 mph (64 km/hr); BIT $= 1s$)

5.1.2 Roll Dynamics in Braking-in-turn Maneuver

The lateral acceleration results for braking-in-turn maneuvers are shown in Figure 14a for 40 mph (64 km/h) initial speed, 50-ft J-turn, and 1s BIT. There is a phase delay in the lateral acceleration responses of the front and rear trailers, with respect to the tractor's lateral acceleration, which in itself is delayed to the applied steering. The lateral acceleration for the rear trailer lags the tractor and front trailer and additionally is smaller than the two. Both the front-to-rear steering lag commonly exists in LCVs and reduction in speed due to braking contribute to this phenomenon.

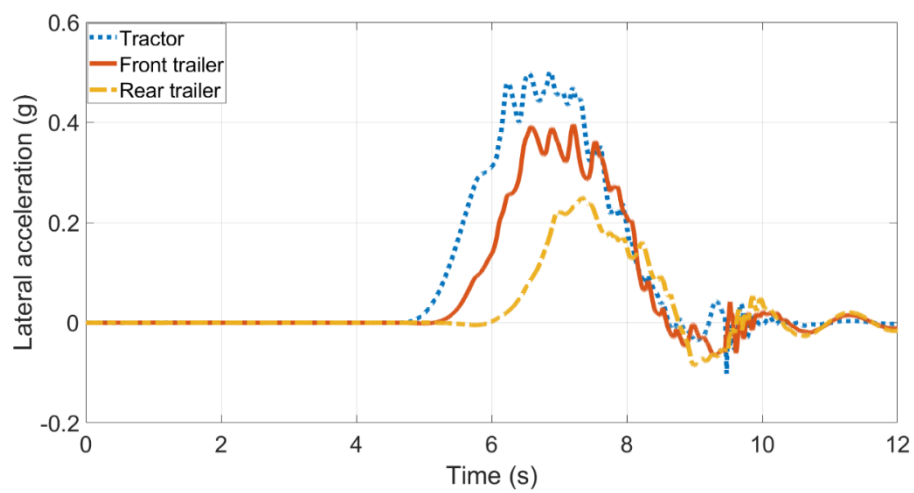

(a)

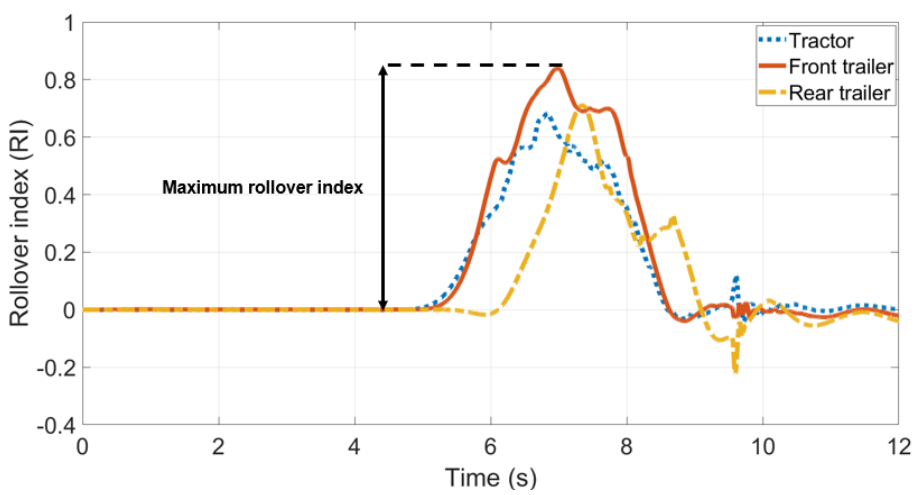

(b)

Figure 14. Time trace of (a) lateral accelerations and (b) rollover index during braking-in-turn (initial speed=40 mph (64 km/hr); BIT $= 1s$)

To quantitatively gauge the likelihood of a rollover, the rollover index (RI) is introduced, calculated as for each axle [45]:

$$RI = \frac{F_{z_R} - F_{z_L}}{F_{z_R} + F_{z_L}} \tag{15}$$

F_{z_R} and F_{z_L} are the tire vertical loads on the right and left. $|RI| = 1$ implies 100% axle weight transfer from one side to the other side, which most likely would lead to wheel lift and possibly rollover. The greater the RI is, the higher is the likelihood of vehicle rollover. The RI=1 is often used as a measure of rollover threshold, which is a relatively conservative metric since wheel lift may not necessarily cause a rollover [46].

The tractor, front trailer, and rear trailer RI are shown in Figure 14b during the braking-in-turn maneuver. The front trailer experiences a larger RI than the tractor due to its higher CG. Additionally, the front trailer RI is larger than the rear trailer because it is subjected to larger lateral accelerations during the cornering and braking maneuver, as discussed previously in Figure 14a. This means that the risk of rollover for the front trailer is higher than the rear trailer in this type of steering and braking. It is important to note that the front trailer lateral acceleration (and its higher likelihood of rollover) do not transfer directly to the tractor and rear trailer due to the dynamics of the pintle hook and the slight free-play that may exist at the hitch-pintle hook interface. The peak RI for the front trailer is used as the metric to assess the likelihood of vehicle rollover.

5.1.3 Yaw Dynamics and Path Deviation in Braking-in-turn Maneuver

The front and rear trailers are delayed relative to the tractor, as shown in Figure 15a, as anticipated. The delay occurs because of the inertial effects and compliances from the front to the rear of the vehicle. The trends are the same as the lateral accelerations in Figure 14a. Another element of risk for LCV is the potential of excessive outward sway of the trailers, as measured by the deviation between the path of the tires on the outside of the turn, as shown in Figure 15b. If the tire deviation is larger than the road space (e.g., lane width plus clearance to a roadside guardrail), the swing can cause a collision and risk of property damage or injury. Using a 2-ft guardrail clearance (the minimum allowed by the U.S. DOT [47]) and 12-ft lane width (the standard lane width for most U.S. roads), no collisions were observed for any of the maneuvers or speeds including the ones that caused RI=1, the rollover threshold. Therefore, path deviations are not discussed any further, for sake of brevity.

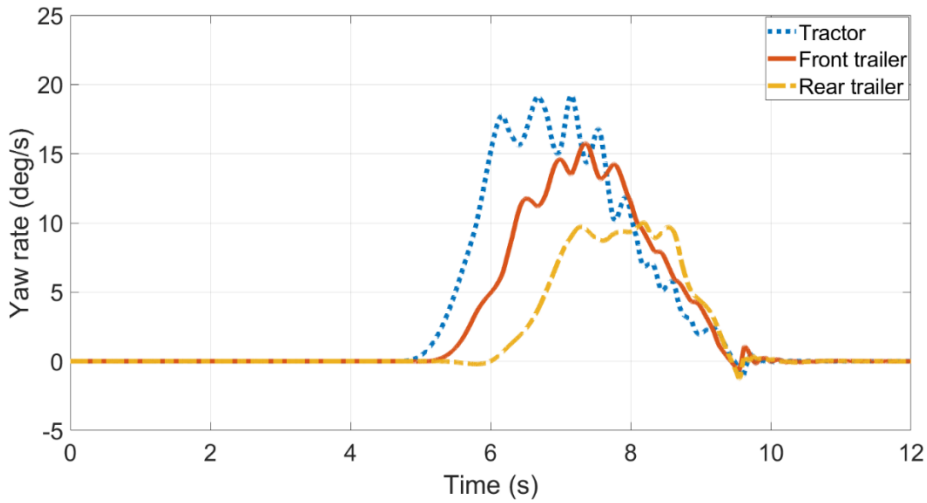

(a)

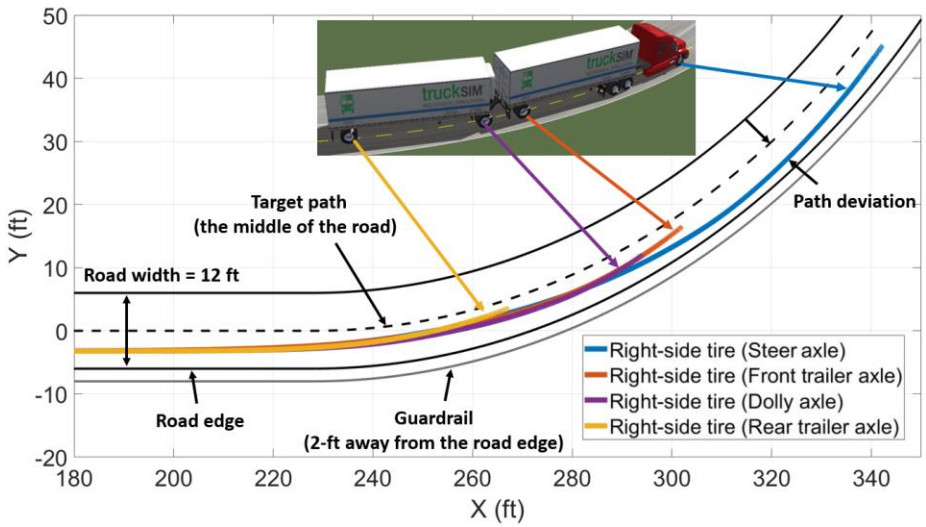

(b)

Figure 15. (a) Time trace of the LCV yaw rates and (b) paths of the tires on the right side of the LCV during the braking-in-turn maneuver (initial speed=40 mph (64 km/hr); BIT $= 1s$)

5.2 Critical Brake Initiation Time (CBIT)

5.2.1 For the Initial Speed of 40 mph (64km/hr)

Based on the preliminary evaluation, simulations with various brake initiation times (BIT) (in 0.05s increments) are performed to determine the critical brake initiation time (CBIT) to avoid rollover. The peak values extracted from the lateral accelerations of the tractor and trailers at different BIT are shown in Figure 16a. As BIT increases (i.e., braking is delayed relative to the start of steering), the tractor and trailers experience larger lateral accelerations because of the larger steering angle and delay in scrubbing speed. At CBIT=1.2s, the front trailer reaches its upper

rollover index (RI) limit of 1, as shown in Figure 16b. This indicates that unless the driver applies the brakes within 1.2s of initiating the turn, the vehicle would be at significantly increased risk of rollover. Although not presented in this paper, the simulation predictions closely match our LCV track testing results.

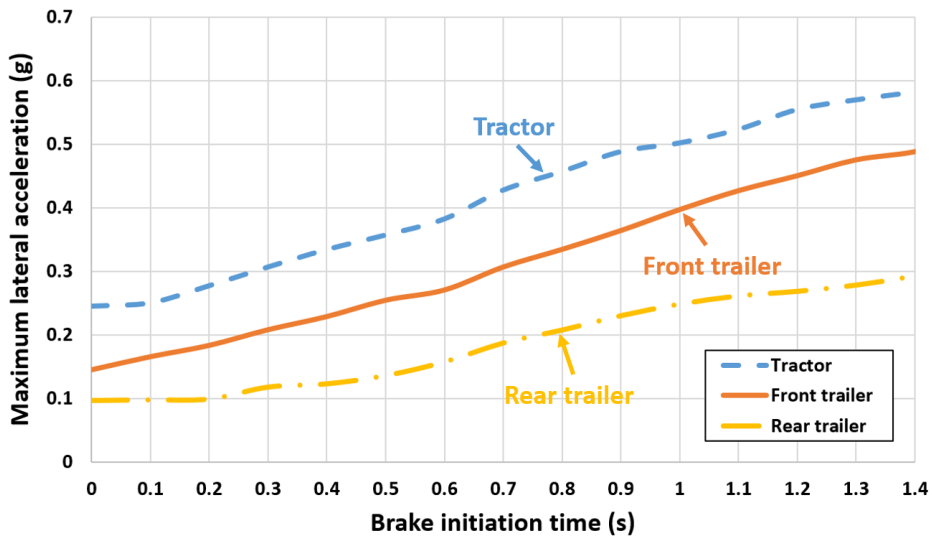

(a)

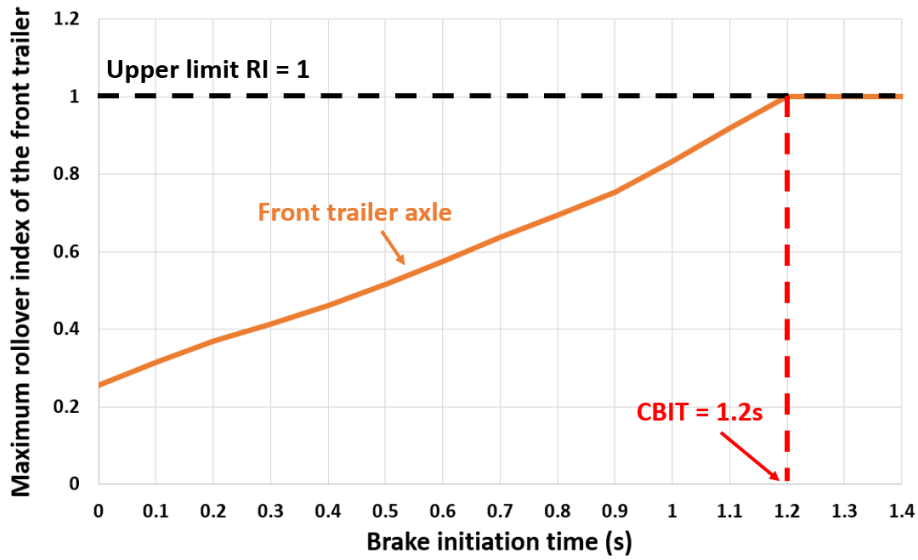

(b)

Figure 16. (a) The maximum lateral accelerations and (b) the maximum rollover index versus the brake initiation time (BIT) for the 150-ft J-turn at initial speed = 40 mph (64 km/hr)

5.2.2 Effect of Speed

Additional simulations are performed for initial speeds ranging from 33 mph (53 km/hr) to 54.5 mph (88 km/hr) (in 0.5-mph (0.8 km/hr) increments), to evaluate the relationship between CBIT

and speed. 33 mph (53 km/hr) is chosen because at speeds lower than that no rollover occurs when the brakes are not applied. The results are summarized in Figure 17. It shows a nonlinear relationship between CBIT and speed. Approximately, as speed increases by 10%, CBIT decreases by 24%. The CBIT decreases to zero at 54.5 mph (88 km/hr), indicating that unless the driver reduces the speed before entering the turn the LCV would be at a significantly increased risk of rollover. The CBIT plot in Figure 17 shows two regions:

- **Region A**: Indicates the combination of initial speeds and braking into the turn that would prevent rollovers. For example, point "a" indicates that at 40 mph (64 km/hr), if braking is initiated at 0.8s after the turn, the rollover can be prevented.
- **Region B**: Indicates the speeds or CBIT that would not prevent a rollover. For example, point "b" indicates that at 40 mph (64 km/hr), if braking is initiated at 1.4s after the turn, the rollover would not be prevented.

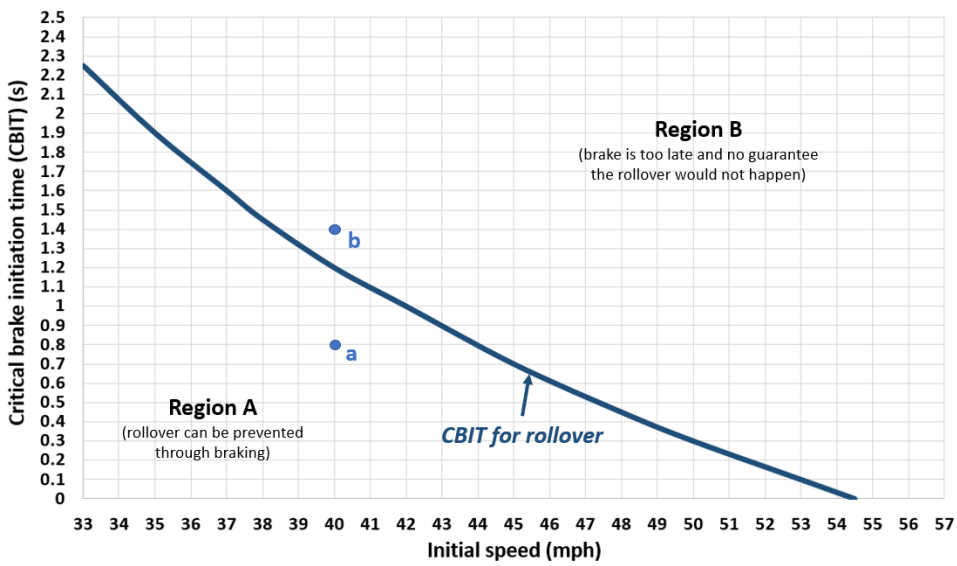

Figure 17. Summary results of critical brake initiation time (CBIT) of rollover for the cases of different initial speeds

Another factor influences the steering and braking dynamics in turns is the cargo load, not surprisingly. As shown in Figure 18, increasing the cargo load lowers the CBIT boundary, indicating that at a given speed CBIT decreases as cargo weight increases. The light, medium, and heavy loads in Figure 18 represent the 8000 lb. (3600 kg), 15000 lb. (6800 kg), and 22000 lb. (10000 kg) of cargo load, respectively. Further details for each load condition are included in Table A2 (Appendix A). As the data indicates, there is far less tolerance for speed in a turn for a

heavily-loaded truck. There is also a smaller time margin for the driver to take action to reduce vehicle speed before it is too late. Hence, more rollover incidents under heavy load conditions.

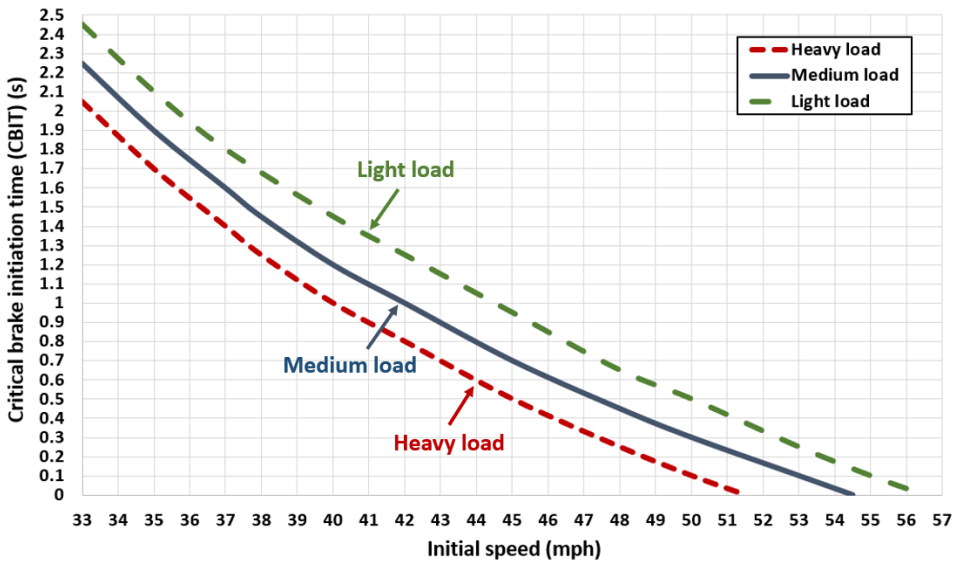

Figure 18. Comparison results of the critical brake initiation time (CBIT) among different loading conditions

6. Conclusions

The relationship between vehicle speed, braking action, and cargo load in rollover dynamics of long combination vehicles (LCV) in a turn were studied, using a 150-ft J-turn. The LCV considered for the study included a semi-tractor, two 33-ft trailers, and a convertor A-dolly, commonly referred to as "33-ft A-doubles." A test-validated co-simulation model in TruckSim® and Simulink® was used for the study to determine the critical brake initiation time (CBIT)—the latest moment the driver can take braking action to prevent a rollover—for various load conditions and speeds. The simulation results indicate that there is a limited amount of time for a driver to intervene with braking in a turn to prevent a rollover. This is caused by an LCV's high CG that increases susceptibility to rollover, and large vehicle length that delays the activation of full braking from the time the driver initiates braking to when the trailers and dolly's brakes are fully engaged. Some of the key findings of this study are:

1. Delayed braking results in larger lateral accelerations, mainly due to speed and raised cargo CG and increased risk of rollover. The CBIT decreases nonlinearly with increased speed. For instance, for a fully-loaded trailer, as speed increases by 25% from 40 mph (64 km/hr) to 50 mph (80 km/hr), CBIT decreases by 90%, from 1.0s to 0.1s.

2. There is a far shorter time for driver intervention at high speeds, such as during highway driving. For heavily-loaded trailers, a rollover could not be prevented in a 150-ft turn by braking intervention at initial speeds of more than 51 mph (82 km/hr).
3. A similar trend as speed is observed for gross weight. As cargo weight increases, CBIT reduces at all speeds. Lighter loads result in longer CBIT, giving the driver more time to intervene through braking to reduce the risk of rollover. An opposite trend is observed for heavier loads. For instance, at 40 mph (64 km/hr), as the cargo load increases by 47%, from 15000 lb. (6800 kg) to 22000 lb. (10000 kg), CBIT decreases by 17%, from 1.2s to 1.0s.

Reference

[1] Y. Chen, A. W. Peterson, C. Zhang, and M. Ahmadian, "A simulation-based comparative study on lateral characteristics of trucks with double and triple trailers," *International journal of vehicle safety,* vol. 11, no. 2, pp. 136-157, 2019.

[2] T. Adams, D. Kleinmaier, A. Marach, G. Helfrich, J. Levine, and J. Bittner, "Longer combination vehicles: an estimation of their benefits and public perception of their use," National Center for Freight and Infrastructure Research and Education (US), 2012.

[3] L. Palkovics, A. Semsey, and E. Gerum, "Roll-over prevention system for commercial vehicles–additional sensorless function of the electronic brake system," *Vehicle System Dynamics,* vol. 32, no. 4-5, pp. 285-297, 1999.

[4] S. D. Green, "PREVENT HEAVY TRUCK ROLLOVER," *Traffic Safety (Chicago),* vol. 2, no. 4, 2002.

[5] F. M. C. S. Administration, "Large Truck and Bus Crash Facts 2018," 2018.

[6] H. L. D. I. Insurance Institute for Highway Safety, "Fatality Facts 2018 Large trucks," 2018. [Online]. Available: https://www.iihs.org/topics/fatality-statistics/detail/large-trucks.

[7] S.-K. Chen, N. Moshchuk, F. Nardi, and J. Ryu, "Vehicle rollover avoidance," *IEEE Control Systems Magazine,* vol. 30, no. 4, pp. 70-85, 2010.

[8] A. G. Nalecz, "Influence of vehicle and roadway factors on the dynamics of tripped rollover," *International Journal of Vehicle Design,* vol. 10, no. 3, pp. 321-346, 1989.

[9] G. Phanomchoeng and R. Rajamani, "New rollover index for the detection of tripped and untripped rollovers," *IEEE Transactions on Industrial Electronics,* vol. 60, no. 10, pp. 4726-4736, 2012.

[10] A. J. McKnight and G. T. Bahouth, "Analysis of large truck rollover crashes," *Traffic injury prevention,* vol. 10, no. 5, pp. 421-426, 2009.

[11] Z. Huang, W. Nie, S. Kou, and X. Song, "Rollover detection and control on the non-driven axles of trucks based on pulsed braking excitation," *Vehicle system dynamics,* vol. 56, no. 12, pp. 1864-1882, 2018.

[12] H. C. Gabler and D. J. Gabauer, "Opportunities for reduction of fatalities in vehicle-guardrail collisions," in *Annual Proceedings/Association for the Advancement of Automotive Medicine*, 2007, vol. 51: Association for the Advancement of Automotive Medicine, p. 31.

[13] C. B. Winkler, "Rollover of heavy commercial vehicles," Society of Automotive Engineers, Warrendale, Pa., 1999.

[14] B.-C. Chen and H. Peng, "Rollover warning for articulated heavy vehicles based on a time-to-rollover metric," 2005.

[15] H. Yu, L. Güvenc, and Ü. Özgüner, "Heavy duty vehicle rollover detection and active roll control," *Vehicle system dynamics,* vol. 46, no. 6, pp. 451-470, 2008.

[16] A. S. Trigell, M. Rothhämel, J. Pauwelussen, and K. Kural, "Advanced vehicle dynamics of heavy trucks with the perspective of road safety," *Vehicle system dynamics,* vol. 55, no. 10, pp. 1572-1617, 2017.

[17] Y. Chen, Zheng, X., Peterson, A., Ahmadian, M., , "Simulation Evaluation on the Rollover Propensity of Multi-trailer Trucks at Roundabouts," *SAE technical paper,* 2020, Art no. 2020-01-5005, doi: 10.4271/2020-01-5005.

[18] U. DoT, "Federal size regulations for commercial motor vehicles," ed: Washington, DC: US Department of Transportation Federal Highway Administration, 2004.

[19] R. R. Knipling, "Twin 33 Foot Truck Trailers: Making U.S. Freight Transport Safer And More Efficient," 2016. [Online]. Available: https://americansformoderntransportation.org/wp-content/uploads/Ron-Knipling-Twin-33-Study-vF.pdf.

[20] G. Morrison and D. Cebon, "Combined emergency braking and turning of articulated heavy vehicles," *Vehicle system dynamics,* vol. 55, no. 5, pp. 725-749, 2017.

[21] A. L. Dunn, G. Heydinger, G. Rizzoni, and D. Guenther, "In-depth analysis of the influence of high torque brakes on the jackknife stability of heavy trucks," *SAE transactions,* pp. 255-272, 2003.

[22] K. J. Seluga, R. M. Obert, and I. U. Ojalvo, "Articulated Vehicle Yaw Stability During Braking–A Parametric Study," *SAE transactions,* pp. 248-255, 2004.

[23] M. Gäfvert and J. Svendenius, "A novel semi-empirical tyre model for combined slips," *Vehicle System Dynamics,* vol. 43, no. 5, pp. 351-384, 2005.

[24] J. Svendenius and M. Gäfvert, "A semi-empirical dynamic tire model for combined-slip forces," *Vehicle System Dynamics,* vol. 44, no. 2, pp. 189-208, 2006.

[25] L. Li, K. Yang, G. Jia, X. Ran, J. Song, and Z.-Q. Han, "Comprehensive tire–road friction coefficient estimation based on signal fusion method under complex maneuvering operations," *Mechanical Systems and Signal Processing,* vol. 56, pp. 259-276, 2015.

[26] L. Shaohua, Y. Shaopu, and C. Liqun, "Investigation on cornering brake stability of a heavy-duty vehicle based on a nonlinear three-directional coupled model," *Applied Mathematical Modelling,* vol. 40, no. 13-14, pp. 6310-6323, 2016.

[27] D. Zhang and B. Tabarrok, "Dynamic modelling and simulation of log-hauling trucks with combined tire-cornering and braking forces," *Multibody System Dynamics,* vol. 4, no. 1, pp. 1-22, 2000.

[28] Y. Chen, A. W. Peterson, and M. Ahmadian, "Achieving anti-roll bar effect through air management in commercial vehicle pneumatic suspensions," *Vehicle System Dynamics,* vol. 57, no. 12, pp. 1775-1794, 2019.

[29] Y. Chen, Y. Hou, A. Peterson, and M. Ahmadian, "Failure mode and effects analysis of dual levelling valve airspring suspensions on truck dynamics," *Vehicle system dynamics,* vol. 57, no. 4, pp. 617-635, 2019.

[30] Y. Chen and M. Ahmadian, "Countering the Destabilizing Effects of Shifted Loads through Pneumatic Suspension Design," *SAE Int. J. Veh. Dyn., Stab., and NVH,* vol. 4, no. 1, pp. 5-17, 2020.

[31] Y. Chen, Z. Zhang, and M. Ahmadian, "Comparative Analysis of Emergency Evasive Steering for Long Combination Vehicles," *SAE Int. J. Commer. Veh,* vol. 13, no. 3, 2020.

[32] Y. Chen, M. Ahmadian, and A. Peterson, "Pneumatically balanced heavy truck air suspensions for improved roll stability," SAE Technical Paper, 0148-7191, 2015.

[33] T. D. Gillespie, *Fundamentals of vehicle dynamics*. Society of automotive engineers Warrendale, PA, 1992.

[34] P. S. Fancher, "Generic data for representing truck tire characteristics in simulations of braking and braking-in-a-turn maneuvers. Final report," 1995.

[35] K. Nam, S. Oh, H. Fujimoto, and Y. Hori, "Estimation of sideslip and roll angles of electric vehicles using lateral tire force sensors through RLS and Kalman filter approaches," *IEEE Transactions on Industrial Electronics,* vol. 60, no. 3, pp. 988-1000, 2012.

[36] L. Balderas, "Representation of truck tire properties in braking and handling studies: the influence of vertical load on side force characteristics. Final report," 1988.

[37] H. Pacejka, *Tire and vehicle dynamics*. Elsevier, 2005.

[38] H. B. Pacejka and E. Bakker, "The magic formula tyre model," *Vehicle system dynamics*, vol. 21, no. S1, pp. 1-18, 1992.

[39] H. B. Pacejka and R. S. Sharp, "Shear force development by pneumatic tyres in steady state conditions: a review of modelling aspects," *Vehicle system dynamics*, vol. 20, no. 3-4, pp. 121-175, 1991.

[40] S. C. Subramanian, S. Darbha, and K. R. Rajagopal, "Modeling the pneumatic subsystem of an S-cam air brake system," *J. Dyn. Sys., Meas., Control*, vol. 126, no. 1, pp. 36-46, 2004.

[41] N. S. Zichen Zhang, Yang Chen, Mehdi Ahmadian, "Detailed Modeling of Pneumatic Braking in Long Combination Vehicles," *SAE Int. J. Commer. Veh*, 2021.

[42] N. H. T. S. Administration, "Federal Motor Vehicle Safety Standards; Air Brake Systems. 49 CFR Part 571, Docket No," NHTSA–2009-0083, 2009.

[43] F. Gross, P. P. Jovanis, and K. Eccles, "Safety effectiveness of lane and shoulder width combinations on rural, two-lane, undivided roads," *Transportation Research Record*, vol. 2103, no. 1, pp. 42-49, 2009.

[44] M. Acosta, S. Kanarachos, and M. Blundell, "Road friction virtual sensing: a review of estimation techniques with emphasis on low excitation approaches," *Applied Sciences*, vol. 7, no. 12, p. 1230, 2017.

[45] M. Ahmadian, "Integrating Electromechanical Systems in Commercial Vehicles for Improved Handling, Stability, and Comfort," *SAE International Journal of Commercial Vehicles*, vol. 7, no. 2014-01-2408, pp. 535-587, 2014.

[46] R. Goldman, M. El-Gindy, and B. Kulakowski, "Rollover dynamics of road vehicles: Literature survey," *International Journal of Heavy Vehicle Systems*, vol. 8, no. 2, pp. 103-141, 2001.

[47] D. o. T. F. H. Administration. "Frequently Asked Questions: Barriers, Terminals, Transitions, Attenuators, and Bridge Railings." https://safety.fhwa.dot.gov/roadway_dept/countermeasures/faqs/qa_bttabr.cfm (accessed 2021).

Abbreviations

LCV	Long combination vehicle	**BIT**	Brake initiation time
FMCSA	Federal Motor Carrier Safety Administration	**CBIT**	Critical brake initiation time
US	United States	**DOF**	Degree of freedom
FMVSS	Federal Motor Vehicle Safety Standards	**OH**	Ohio
CG	Center of gravity	**CAD**	Computer-aided design
DOT	Department of Transportation	**TRC**	Transportation Research Center
ABS	Anti-lock braking system	**RI**	Rollover index
GPS	Global positioning system		

Appendix A

Table A1. Parameters for the 33-ft A-double dynamic simulation

Tractor			
Sprung weight	15882 lb.	Drive axle roll inertia	14350 lb·ft^2
Roll moment of inertia	168435 lb·ft^2	Tire unloaded radius (drive axle)	20.9 in
Pitch moment of inertia	515530 lb·ft^2	Tire vertical stiffness (drive axle)	4411 lb./in
Yaw moment of inertia	511932 lb·ft^2	Airspring effective area (drive axle)	70 in^2
Wheelbase	255 in	Airspring initial height (drive axle)	11 in
Steer axle track	77 in	Damper lateral span (steer axle)	43.5 in
Drive axle track	77 in	Spring lateral span (steer axle)	32.5 in
Long. distance from CG to steer axle	127.0 in	Damping coefficient (steer axle)	85.6 lb-s/in
Long. distance from CG to rear drive axle	153.0 in	Leaf spring stiffness (steer axle)	1016.4 lb./in
Long. distance from CG to front drive axle	102.8 in	Damper lateral span (drive axle)	30 in
Long. distance from CG to fifth wheel	131.2 in	Spring lateral span (drive axle)	42 in
Fifth wheel's roll angle limit	± 2 deg	Damping coefficient (drive axle)	164.7 lb-s/in
Steer axle roll inertia	7950 lb·ft^2	Steering ratio	22.5 deg/deg
Tire unloaded radius (steer axle)	20.7 in	Steer axle unsprung weight	1256 lb.
Tire vertical stiffness (steer axle)	4407 lb./in	Drive axle unsprung weight	1410 lb.
Wheel spin moment of inertia	330 lb·ft^2	CG height to the ground	39.8 in
Fifth wheel height to the ground	47 in	Dual tire lateral spacing	12 in
Semi-trailer			
Trailer tare weight	10110 lb.	Long. distance from CG to kingpin	171.1 in
Roll moment of inertia	403219 lb·ft^2	Long. distance from CG to pintle hitch	193.9 in
Pitch moment of inertia	2990579 lb·ft^2	Loaded trailer weight	25110 lb.
Yaw moment of inertia	2913493 lb·ft^2	Damper lateral span	31 in
CG height to the ground	79.5 in	Spring lateral span	39 in
Dual tire lateral spacing	12 in	Axle roll inertia	14350 lb·ft^2
Wheelbase	331 in	Damping coefficient	285.5 lb-s/in
Axle Track	77 in	Axle unsprung weight	1410 lb.
Tire unloaded radius	20.5 in	Tire vertical stiffness	4411 lb./in
Airspring effective area	80 in^2	Airspring initial height	8 in
Wheel spin moment of inertia	330 lb·ft^2	Kingpin height to the ground	47 in
Pintle hitch height to the ground	33 in		
Dolly			
Sprung weight	1527 lb.	Dual tire lateral spacing	144 in
Long. distance from CG to kingpin	31.5 in	Damper lateral span	34 in
Long. distance from CG to fifth wheel	40.5 in	CG height to the ground	35.4 in
Roll moment of inertia	28488 lb·ft^2	Axle roll inertia	14350 lb·ft^2
Pitch moment of inertia	35612 lb·ft^2	Spring lateral span	31 in
Yaw moment of inertia	41663 lb·ft^2	Airspring initial height	14 in
Wheelbase	72 in	Damping coefficient	164.7 lb-s/in
Airspring effective area	70 in^2	Tire unloaded radius	20.5 in
Wheel spin moment of inertia	330 lb·ft^2	Axle unsprung weight	1410 lb.
Fifth wheel height to the ground	47 in	Axle Track	77 in
Fifth wheel roll angle limit	± 2 deg		

Table A2. Parameters of the 33-ft trailer for the different load conditions

Parameter	**Heavy Load**	**Medium Load**	**Light Load**
Cargo weight	22000 lb.	15000 lb.	8000 lb.
Loaded trailer weight	32100 lb.	25100 lb.	18100 lb.
CG height to the ground	83.5 in	79.5 in	75.1 in
CG longitudinal distance to the kingpin	180.1 in	183.5 in	189.6 in
Sprung mass roll moment of inertia	424759 lb·ft^2	350130 lb·ft^2	271774 lb·ft^2
Sprung mass pitch moment of inertia	3352215 lb·ft^2	2727101 lb·ft^2	2096537 lb·ft^2
Sprung mass yaw moment of inertia	3300658 lb·ft^2	2677054 lb·ft^2	2051726 lb·ft^2
Load fill	80%	80%	80%
Load volume	1900 ft^3	1900 ft^3	1900 ft^3
Load density	11.6 lb./ft^3	7.9 lb./ft^3	4.2 lb./ft^3

Appendix B

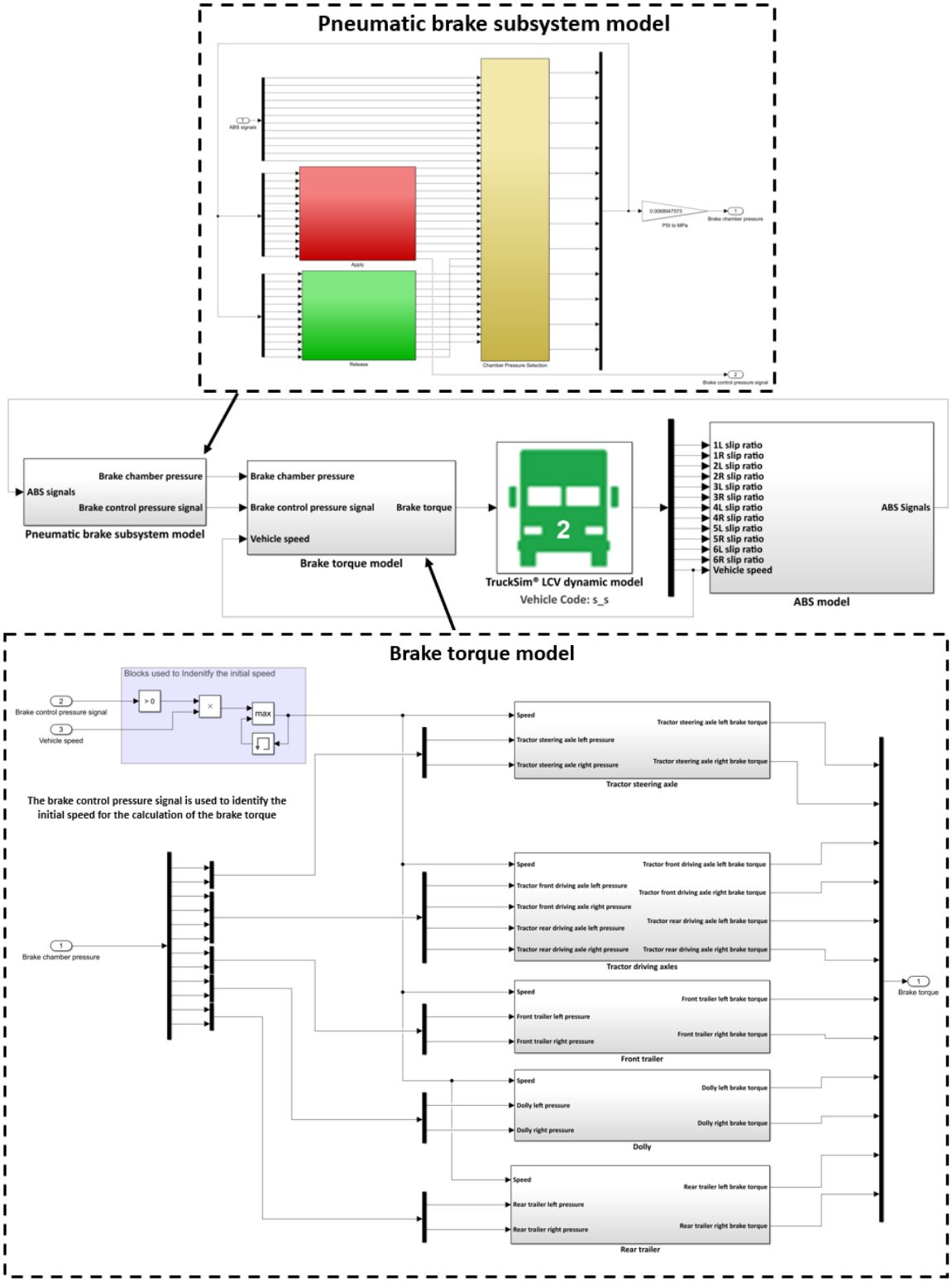

Figure B1. Co-simulation model of pneumatic-brake and vehicle-dynamics in Simulink®